Nanoparticles

Deutsche Ausgabe: DOI: 10.1002/ange.201604710
Internationale Ausgabe: DOI: 10.1002/anie.201604710

In Situ Single-Nanoparticle Spectroscopy Study of Bimetallic Nanostructure Formation

*Jeremy G. Smith+, Indranath Chakraborty+, and Prashant K. Jain**

Abstract: *Bimetallic nanostructures (NSs), with utility in catalysis, are typically prepared using galvanic exchange (GE), but the final catalyst morphology is dictated by the dynamics of the process. In situ single nanoparticle (NP) optical scattering spectroscopy, coupled with ex situ electron microscopy, is used to capture the dynamic structural evolution of a bimetallic NS formed in a GE reaction between Ag and* $[PtCl_6]^{2-}$*. We identify an early stage involving anisotropic oxidation of Ag to AgCl concomitant with reductive deposition of small Pt clusters on the NS surface. At later stages of GE, unreacted Ag inclusions phase segregate from the overcoated AgCl as a result of lattice strain between Ag and AgCl. The nature of the structural evolution elucidates why multi-domain Ag/AgCl/Pt NSs result from the GE process. The complex structural dynamics, determined from single-NP trajectories, would be masked in ensemble studies due to heterogeneity in the response of different NPs.*

While transition-metal nanoparticles (NPs) have been quite popular in heterogeneous catalysis, there is a growing interest in NPs with bimetallic composition. Bimetallic compositions often exhibit properties unique from those of the component metals[1,2] either due to geometric strain or the so-called "ligand" environment effect resulting from the formation of heteroatom bonds. In other cases, bimetallic compositions allow the synergy between the two metals to be exploited. Galvanic exchange (GE) is a popular method for preparing bimetallic nanostructures with high specific surface area.[3–6] Formation of Ag/Pt nanostructures[3,5,7,8] through the galvanic exchange of Ag NPs by $[PtCl_6]^{2-}$, studied herein, is a good example. Electronic and catalytic properties of a bimetallic nanostructures are not determined by the molar composition alone; spatial distribution of the metals also matters.[9] Therefore, it is crucial to understand what dictates morphologies of bimetallic nanostructures formed via galvanic exchange.

Galvanic exchange of Ag with $[PtCl_6]^{2-}$ studied herein results in complex structures consisting of Pt clusters deposited on AgCl with phase-separated Ag domains. These structures have utility for catalytic and photocatalytic studies because of the catalytically active nature of Pt clusters and the ability of Ag to enhance plasmonic excitation and surface-enhanced Raman scattering (SERS), providing a platform for probing of surface adsorption and reactions occurring on Pt active sites.[10,11] The insulating AgCl serves to prevent undesirable electronic/chemical interactions between the Pt catalyst and the plasmonic Ag reporter.

The formation of multidomain Ag/AgCl/Pt nanostructures is quite unlike the classic Ag to Au galvanic exchange reaction which yields porous Ag/Au alloy nanostructures.[4] To obtain a rationale for the surprising outcome in the Ag–Pt system, we performed in situ studies, from which we determined that the complex Ag/AgCl/Pt morphology is the result of a dynamic sequence of structural steps in the galvanic exchange reaction. Dynamics, which are otherwise hidden in ensemble-level studies,[12–16] are captured by in situ plasmonic spectroscopy of single Ag NPs undergoing galvanic exchange. Single-nanoparticle studies also reveal differences in the trajectories of individual NPs undergoing galvanic exchange. These different classes of behavior serve to explain the heterogeneity in morphology of the formed bimetallic nanostructures. In summary, our studies demonstrate that structural outcomes in galvanic exchange-based nanostructure preparations are dictated by dynamic pathways rather than by thermodynamic considerations; understanding these pathways can aid in better synthetic control necessary for preparing catalysts.

Morphologies and compositions of nanostructures (Figure 1) formed by galvanic exchange of Ag NPs with $[PtCl_6]^{2-}$ were first examined by scanning transmission electron microscopy (STEM) and energy dispersive spectroscopy (EDS). As galvanic exchange progressed, the relative Pt and Cl content of the nanostructure increased, as seen from EDS spectra and expected as per the reaction in Equation (1):

$$4\,Ag_{(s)} + [PtCl_6]^{2-}{}_{(aq)} \rightarrow Pt_{(s)} + 4\,AgCl_{(s)} + 2\,Cl^-{}_{(aq)} \qquad (1)$$

NPs begin (Figure 1 A–D) with relatively uniform shape (spherical) and size (46 ± 8 nm). At initial stages of galvanic exchange, Ag NPs show pitting (Figure 1 E,F), with pits partially filled with AgCl (Figure 1 H). Further galvanic exchange results in expansion of existing pits and associated AgCl regions, and formation of new ones (Figure 1 I,J). In STEM images, the AgCl corresponds to regions of lower contrast as confirmed by AgCl crystallographic reflections present in electron diffraction patterns, particularly at the

---

[*] J. G. Smith,[+] Dr. I. Chakraborty,[+] Prof. P. K. Jain
Dept. of Chemistry
University of Illinois at Urbana-Champaign
600 South Mathews Avenue, Urbana, IL 61801 (USA)
E-mail: jain@illinois.edu
Prof. P. K. Jain
Materials Research Lab, University of Illinois at Urbana-Champaign
104 South Goodwin Avenue, Urbana, IL 61801 (USA)

[+] These authors contributed equally to this work.

Supporting information and the ORCID identification number(s) for the author(s) of this article can be found under http://dx.doi.org/10.1002/anie.201604710.

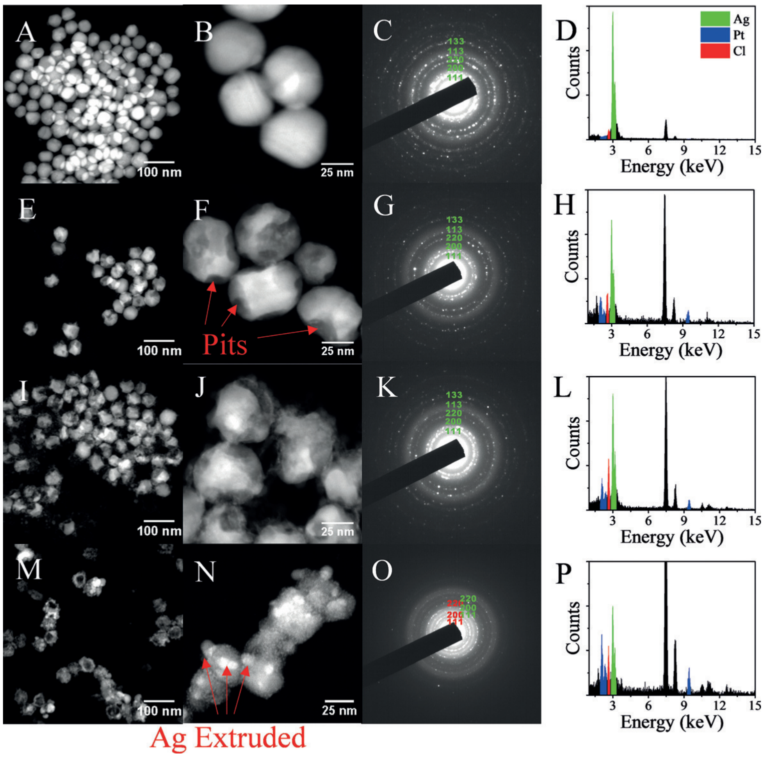

Figure 1. A,B,E,F,I,J,M,N) High-angle annular dark-field (HAADF) STEM images of nanostructures at various stages (top to bottom) in the galvanic exchange of Ag NPs with $[PtCl_6]^{2-}$. These samples at different stages were prepared via an ensemble titration as detailed in Figure S5. C,G,K,O) Electron diffraction patterns show nanostructures contain primarily Ag (diffraction ring indices labeled in green) at all stages, except for the most exchanged sample (O), for which AgCl is a major component (diffraction ring indices labeled in red). D,H,L,P) Wide-field EDS spectra of the nanostructure samples.

final stage of galvanic exchange (Figure 1O), as well as high resolution transmission electron microscopy images (Figure S7). Pt is deposited in the form of small clusters over the entire nanostructure (Figure S7 in the Supporting Information). At the final stage, a large fraction (61%, Table S1) of the nanostructures are composed predominantly of AgCl, with Pt clusters deposited across the surface (Figure S7). A significant fraction (39%, Table S1) of AgCl/Pt nanostructures exhibit, at or near their surfaces, sizable (> 10 nm) Ag domains identified from their higher contrast (Figure 1M,N). These domains are surprising under the expectation that the galvanic exchange reaction proceeds via a shrinking core model.

While the ex situ study (Figure 1) provided snapshots of the structural outcomes in the reaction, the study is unable to track the dynamics of the restructuring processes that lead to these structures. An in situ single-NP-level study elucidates the structural dynamics and the cause of formation of multi-domain Ag/AgCl/Pt nanostructures. We monitored kinetics of galvanic exchange by in situ dark-field scattering spectroscopy of individual Ag NPs subject to a flow of $K_2Pt(IV)Cl_6$ solution (Figure 2). Due to the strong localized surface plasmon resonance (LSPR) of the 46 nm Ag NPs, their scattering cross-section is large enough to allow single NP level sensitivity in dark-field scattering.[17–22] Whereas Ag has inter-band transitions in the UV region of the spectrum, deposited Pt has strong d→sp transitions in the visible region. Moreover, formed AgCl is a high refractive index (RI) dielectric. As a result, the

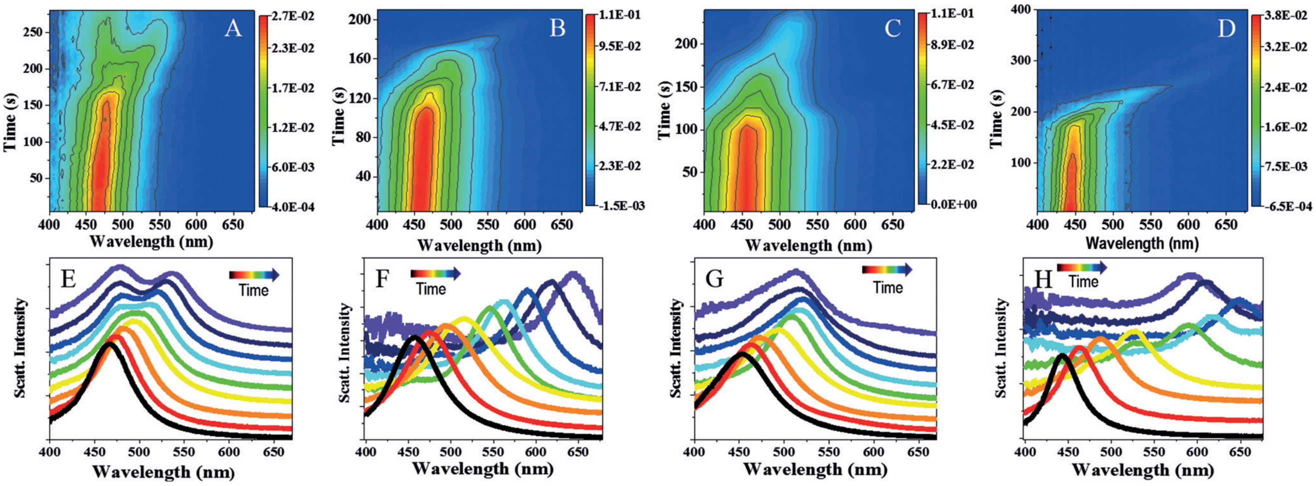

Figure 2. In situ spectral monitoring of single nanoparticles undergoing galvanic exchange with $[PtCl_6]^{2-}$. A,B,C,D) Color contour plots of scattering intensity versus wavelength (*x*-axis) and time (*y*-axis) for four representative individual Ag NPs, showing how the LSPR scattering spectrum evolves in the course of galvanic exchange in a 50 μM K_2PtCl_6 solution flowing at a rate of 1.5 mL h^{-1}. Individual NPs display one of three different spectral behaviors: LSPR red shift and subsequent peak splitting (A), continuous red shift only (B), and LSPR red-shift followed by a blue shift (C,D). K_2PtCl_6 solution enters the flow cell at $t \approx 90$ s (for A and D) and $t \approx 80$ s (for B and C). Spectra were collected with a 5 s integration time. E,F,G,H) Spectra from select times from the respective contour plots are shown in a normalized form to accentuate spectral features. For clarity, the low signal-to-noise (S/N) spectra at higher reaction times were smoothed by the Saviztky-Golay method using a 5 point window (see Figure S3 for unprocessed spectra and times at which the selected spectra were acquired). Contour plots for all 55 NPs studied are shown in Figure S4 and the observed spectral behaviors are summarized in Table S1.

LSPR of the hybrid nanostructure formed in galvanic exchange is damped and spectrally shifted relative to that of the starting Ag NP. The exact spectral progression between end states depends on the nature of the structural evolution.[10,23–26] Discrete dipole approximation (DDA) simulations of LSPR spectra,[27] guided by observations from ex situ STEM, allowed us to assign the spectral evolution observed in situ to the kinetic sequence of structural and compositional changes occurring in the galvanic exchange process.

Scattering intensity trajectories of individual NPs undergoing galvanic exchange appear similar to one another and therefore to the ensemble-averaged trajectory (Figure S1). However, spectral monitoring of individual NPs reveals NP-to-NP heterogeneities (Figure 2). For every NP studied, the LSPR spectrum undergoes a red-shift at early times. This red-shift has two origins, as will be confirmed later with simulations. First, the increased RI of AgCl (2.06) relative to the surrounding solution (1.33) leads to an increase in the net RI of the environment surrounding the Ag NP. The second cause is the non-isotropic manner in which the Ag NP is pitted in the reaction.

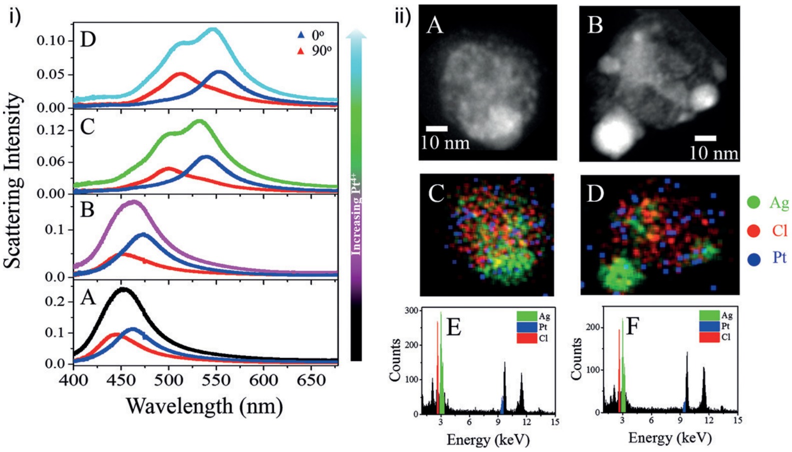

Figure 3. i) A–D) Evolution of polarization-dependence of LSPR spectrum of a representative nanostructure in the course of galvanic exchange. Spectra for orthogonal polarization directions indicated as 0° and 90° and the unpolarized spectrum are shown. ii) Morphologies and compositions of two representative nanostructures (left and right) obtained from galvanic exchange (same sample as the one shown in Figure 1 M–P, Figure S6 I–L, and blue curve in Figure S5 B). HAADF-STEM images (A,B) show nanostructures contain higher contrast domains of 10–25 nm size. Elemental mapping (C,D) shows these regions are enriched in Ag (green), and depleted in Cl (red). Pt (blue) is distributed ubiquitously across the nanostructure. EDS spectra (E,F) of the entire nanostructure indicate a composition of 15, 80, and 5 % w/w Cl, Ag, and Pt, respectively (left) and 15, 81, and 4 % w/w right).

Later in the reaction, NPs begin to diverge in terms of their spectral behavior. Three different classes of behavior are seen (Figures 2, and Figures S3,S4). Statistics for prevalence of these behaviors is summarized in Table S1. Spectra of several NPs (class 1) simply continue to red-shift with time (Figure 2 B,F; Figure S4 labeled R). However, a fraction of NPs (class 2, ca. 44 % of cases) display peak-splitting, the degree of which gradually increases along the reaction trajectory (Figure 2 A,E; Figure S4 labeled RS). Presence of split peaks does not always persist throughout the trajectory; in some cases, split peaks revert back at later times to a single, red-shifted peak. A fraction of the NPs (class 3, ca. 33 %), after having proceeded through a stage of considerable LSPR red-shift, with or without peak-splitting, begin to show a blue-shift (Figure 2 C,D,G,H; Figure S4 labeled RB) at very late stages in the reaction.

For representative individual nanostructures, we measured the polarization dependence of the LSPR scattering spectrum at four (arrested) stages of galvanic exchange (Figure 3 i). Polarization anisotropy of the nanostructure was found to increase over the course of galvanic exchange, indicating that spectral splitting was caused by the development of structural anisotropy. The initial Ag NP is largely isotropic, as a result of which it exhibits a mostly single-peaked spectrum (Figure 3 i A). But after a small degree of galvanic exchange, the spectrum of the NP splits into two modes corresponding to two orthogonal polarizations.

Taking a cue from the morphology of partially exchanged nanostructures seen in STEM (Figure 1 E,F), we hypothesize that anisotropy originates from localized Ag to AgCl conversion (pitting), as confirmed by a DDA simulation (Figure 4). For a NP with pitting confined around two locations along a selected axis, the simulated LSPR scattering spectrum is significantly red-shifted from the spectrum of the initial Ag NP. Moreover, the LSPR spectrum of the pitted nanostructures is strongly polarization dependent (gold and purple curves in Figure 4 B). In analogy with anisotropic ellipsoidal/rod-like nanostructures,[28] the LSPR mode polarized perpendicular to the pitting axis is significantly red shifted compared to the mode polarized along the pitting axis. When the AgCl domains are made larger (Figure 4 C), splitting increases, thereby capturing the progression of pitting being probed by in situ experiments (Figure 2 E). In the simulated spectrum in Figure 4 C, the lower energy mode is red-shifted as much as 80 nm from the higher energy mode, similar to the observed degree of splitting on a representative single NP in experiments (Figure 2 E).

Additional simulations (Figure 4 D) show that further pitting around locations along the axis perpendicular to the initial pitting axis removes anisotropy: peak splitting is no longer present; the single LSPR mode of the nanostructure is significantly red-shifted compared to the initial NP LSPR. The ca. 100 nm simulated red-shift is consistent with the observed magnitude of spectral shifts in in situ experiments. Simulations in Figure 4 D represent class 1 behavior where no splitting is seen or where initial splitting (class 2) is reversed. In these cases, pitting occurs at several random locations on the NP. The resulting pitted nanostructure has little anisotropy: no LSPR splitting is seen, but only large LSPR red-shifts result from a combination of roughening and AgCl deposition. Alternatively, it is possible that the pitted nanostructure, despite being anisotropic, has its pitting axis perpendicular to the plane of observation, in which case no spectral splitting would be observed.

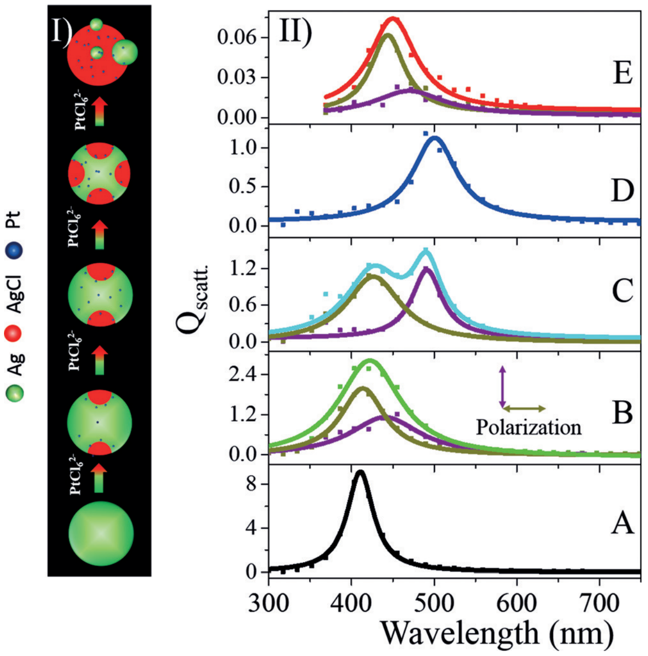

Figure 4. I) Schematic and II) corresponding simulated scattering spectra for an unreacted 51 nm spherical Ag NP (A), an Ag NP that has undergone an anisotropic reaction to form two AgCl domains (red) (B) and (C), but with the extent of pitting greater in (C), an Ag NP with four even larger, isotropically located AgCl domains (D) and a final nanostructure consisting of a 51 nm AgCl NP with three phase-segregated Ag domains of size 20, 10, and 10 nm (E). Scattering spectra for the two orthogonal polarization directions indicated by double-headed arrows were calculated separately and then averaged to generate unpolarized spectra. Pt deposition was not included in these simulations, because small Pt deposits did not cause any spectral shifts but simply damped the LSPR (Figure S8).

Next, we investigated the origin of the late-stage blue-shift observed for class 3 NPs. As noted earlier, almost a third of the nanostructures obtained from galvanic exchange consisted of Ag domains (10–20 nm in size) that had phase segregated from the overcoated AgCl matrix (Figure 1 N). Based on representative morphologies (shown in Figure 3 ii; Figure S7 E–G), we simulated the spectrum of a structure consisting of three spherical Ag domains located on the surface of an AgCl particle (Figure 4 E). The calculated spectrum is blue-shifted as much as 50 nm relative to spectrum of the most pitted nanostructure. This simulated blue-shift is close in magnitude to the maximum blue-shift of 58 nm (Table S1) observed in experiments. Blue-shifts occur because the migration of the Ag domain/s from the interior of the overcoated AgCl matrix to the surface results in the reduction in the effective RI experienced by the Ag domain, the plasmonic scattering center. Thus, blue-shifts observed in situ are a result of the phase segregation of Ag from AgCl seen at the late stages of galvanic exchange. The fraction of cases in which a late-stage blue-shift is seen (33 %) is similar to the fraction of nanostructures that exhibit phase-segregated Ag domains in STEM images (39 %).

It must be noted that the blue shift was not found to be a result of some loss of anisotropy at later stages, such as would arise from additional pitting of an initially anisotropically pitted NP (Figure 4 C,D). As one goes from the anisotropic structure in Figure 4 C to the isotropic one in Figure 4 D, the simulated spectrum is even further red-shifted. This is because the net refractive index increase resulting from AgCl formation dominates over the spectral effect of anisotropy loss. Secondly, we ensured that the blue-shift was not the result of Pt deposition. Pt has a smaller value of the real part of the dielectric function than Ag at visible frequencies, therefore Pt deposition is a potential source of blue-shift; but simulations (Figure S8 C) ruled out this possibility. Even for a simulated structure with Pt deposition significantly over-exaggerated compared to that observed in STEM, the overall blue-shift is significantly smaller in magnitude than the average blue-shift of 15 nm (Table S1) observed at late stages in the in situ experiment.

From the above combination of in situ single-NP spectroscopy, ex situ STEM imaging, and DDA simulations on model morphologies observed in STEM, we delineate in Figure 4 I, the dynamic sequence of structural processes occurring in the galvanic exchange of Ag NPs (A) with $[PtCl_6]^{2-}$. These include pitting accompanied by AgCl formation (B), pit and AgCl domain expansion (C), additional pitting (D), and Ag phase segregation (E). Pt deposition accompanies steps A–D. As seen from the first-order kinetics in K_2PtCl_6 (Figure S2), the rate of the galvanic exchange transformation of the NP is limited by the elementary step involving the reductive breakdown of $[PtCl_6]^{2-}$ to form small Pt clusters and the simultaneous conversion of Ag to AgCl. The loss of Ag and growth of AgCl appears to be selectively localized to already pitted regions (Figure 1 E,F). We believe this is due to the large lattice mismatch of approximately 36 % between Ag (4.09 Å) and AgCl (5.55 Å) and the consequent instability of the Ag/AgCl interface. At an advanced stage, the formed AgCl, being an insulator, disrupts electrochemical contact between the Ag surface and the $[PtCl_6]^{2-}$ solution at the already reacted regions, leading to initiation of Ag pitting and Pt deposition in new locations (Figure 4 D). At this stage (Figure 4 E), the Ag, which is under considerable lattice strain from the overcoated AgCl, spontaneously phase segregates to the surface, where it forms one or more domains. In the around 10 nm size regime, Ag crystallites display liquid-like mobility,[29] which could allow such a major reorganization to occur at room temperature. In instances, where no separate Ag domains are seen to have formed in STEM, it is possible that the segregated Ag domains have reacted further with $[PtCl_6]^{2-}$.

In situ spectroscopy of single Ag NPs undergoing galvanic exchange allowed us to capture the rich dynamic structural evolution of the nanostructure in the course of galvanic exchange. A wealth of structural transformations were identified, including Pt cluster deposition, localized pitting of Ag to form AgCl, AgCl domain growth, electrochemical insulation of Ag from the solution by deposited AgCl, and strain-induced phase segregation of Ag domains from the formed AgCl. The nature of the structural dynamics provides a clear rationale into the complex and unique structural outcome in the Ag–Pt system. Such single-nanoparticle-level insights into the complex dynamics of a seemingly simple reaction, which would otherwise be masked by heterogeneity in ensemble studies, may enable more generally the understanding and control of 1) outcomes of bifunctional Pt-containing nanocatalyst preparations and 2) catalyst restructuring in corrosive/reactive environments.

Acknowledgements

We acknowledge financial support through an Arnold and Mabel O. Beckman Foundation Young Investigator Award. This work was carried out in part at the Frederick Seitz Materials Research Laboratory.

Keywords: alloys · catalysis · nanoscience · plasmon · single-molecule spectroscopy

How to cite: *Angew. Chem. Int. Ed.* **2016**, *55*, 9979 – 9983
Angew. Chem. **2016**, *128*, 10133 – 10137

[1] E. R. Essinger-Hileman, D. DeCicco, J. F. Bondi, R. E. Schaak, *J. Mater. Chem.* **2011**, *21*, 11599 – 11604.
[2] L. E. Marbella, D. M. Chevrier, P. D. Tanchini, O. Shobayo, A. M. Smith, K. A. Johnston, C. M. Andolina, P. Zhang, G. Mpourmpakis, J. E. Millstone, *J. Am. Chem. Soc.* **2015**, *137*, 15852 – 15858.
[3] J. Chen, B. Wiley, J. McLellan, Y. Xiong, Z. Y. Li, Y. Xia, *Nano Lett.* **2005**, *5*, 2058 – 2062.
[4] Y. Sun, B. T. Mayers, Y. Xia, *Nano Lett.* **2002**, *2*, 481 – 485.
[5] S. E. Skrabalak, L. Au, X. Li, Y. Xia, *Nat. Protoc.* **2007**, *2*, 2182 – 2190.
[6] C. Zhou, X. Jiang, L. Yang, Y. Yin, M. Jin, *ChemSusChem* **2013**, *6*, 1883 – 1887.
[7] P. J. Straney, L. E. Marbella, C. M. Andolina, N. T. Nuhfer, J. E. Millstone, *J. Am. Chem. Soc.* **2014**, *136*, 7873 – 7876.
[8] X. Xia, Y. Wang, A. Ruditskiy, Y. Xia, *Adv. Mater.* **2013**, *25*, 6313 – 6332.
[9] E. J. Coleman, A. C. Co, *J. Catal.* **2014**, *316*, 191 – 200.
[10] E. M. Larsson, C. Langhammer, I. Zorić, B. Kasemo, *Science* **2009**, *326*, 1091 – 1094.
[11] E. M. Larsson, M. E. M. Edvardsson, C. Langhammer, I. Zorić, B. Kasemo, *Rev. Sci. Instrum.* **2009**, *80*, 125105.
[12] N. M. Andoy, X. Zhou, E. Choudhary, H. Shen, G. Liu, P. Chen, *J. Am. Chem. Soc.* **2013**, *135*, 1845 – 1852.
[13] K. S. Han, G. Liu, X. Zhou, R. E. Medina, P. Chen, *Nano Lett.* **2012**, *12*, 1253 – 1259.
[14] W. Xu, J. S. Kong, Y.-T. E. Yeh, P. Chen, *Nat. Mater.* **2008**, *7*, 992 – 996.
[15] A. J. Wilson, K. A. Willets, *Nano Lett.* **2014**, *14*, 939 – 945.
[16] S. Thota, S. Chen, Y. Zhou, Y. Zhang, S. Zou, J. Zhao, *Nanoscale* **2015**, *7*, 14652 – 14658.
[17] C. Sönnichsen, T. Franzl, T. Wilk, G. von Plessen, J. Feldmann, *Phys. Rev. Lett.* **2002**, *88*, 077402 – 1 – 077402 – 4.
[18] A. E. Schlather, N. Large, A. S. Urban, P. Nordlander, N. J. Halas, *Nano Lett.* **2013**, *13*, 3281 – 3286.
[19] L. J. Sherry, R. Jin, C. A. Mirkin, G. C. Schatz, R. P. Van Duyne, *Nano Lett.* **2006**, *6*, 2060 – 2065.
[20] A. Tcherniak, S. Dominguez-Medina, W. S. Chang, P. Swanglap, L. S. Slaughter, C. F. Landes, S. Link, *J. Phys. Chem. C* **2011**, *115*, 15938 – 15949.
[21] S. Sheikholeslami, Y. W. Jun, P. K. Jain, A. P. Alivisatos, *Nano Lett.* **2010**, *10*, 2655 – 2660.
[22] J. Olson, S. Dominguez-Medina, A. Hoggard, L.-Y. Wang, W.-S. Chang, S. Link, *Chem. Soc. Rev.* **2015**, *44*, 40 – 57.
[23] I. Zorić, B. Kasemo, C. Langhammer, M. Zaaach, *ACS Nano* **2011**, *5*, 2535 – 2546.
[24] P. K. Jain, X. Huang, I. H. El-Sayed, M. A. El-Sayed, *Acc. Chem. Res.* **2008**, *41*, 1578 – 1586.
[25] C. Langhammer, I. Zorić, B. Kasemo, B. M. Clemens, *Nano Lett.* **2007**, *7*, 3122 – 3127.
[26] C. Novo, A. M. Funston, P. Mulvaney, *Nat. Nanotechnol.* **2008**, *3*, 598 – 602.
[27] P. K. Jain, N. Sobh, J. G. Smith, A. N. Sobh, S. L. White, J. A. Faucheaux, J. Feser, "nanoDDSCAT," DOI: 10.4231/D30P0WS03 can be found under https://nanohub.org/tools/dda, **2016**.
[28] N. R. Jana, L. Gearheart, C. J. Murphy, *J. Phys. Chem. B* **2011**, *115*, 4065 – 4067.
[29] J. Sun, L. He, Y.-C. Lo, T. Xu, H. Bi, L. Sun, Z. Zhang, S. X. Mao, J. Li, *Nat. Mater.* **2014**, *13*, 1007 – 1012.

Received: May 14, 2016